Research Square

Preprints are preliminary reports that have not undergone peer review. They should not be considered conclusive, used to inform clinical practice, or referenced by the media as validated information.

# Effect of metallic Sn addition on the high-voltage discharge performance of $NiF_2$ cathodes for thermal batteries

**Minghao Sun**
Shenyang Ligong University
**Shaohua Yang**
Shenyang Ligong University
**Hongxing Wang**
Shenyang Ligong University
**Zhonghua Du**
duzhonghua@aliyun.com

Shenyang Ligong University

**Research Article**

**Keywords:** thermal battery, $NiF_2$ cathode, metallic Sn, conductive additive, high-voltage discharge

**Posted Date:** October 7th, 2026

**DOI:** https://doi.org/10.21203/rs.3.rs-11110802/v1

**License:** This work is licensed under a Creative Commons Attribution 4.0 International License. Read Full License

**Additional Declarations:** No competing interests reported.

# Abstract

Nickel fluoride ($NiF_2$) is an attractive cathode candidate for thermal batteries because of its relatively high discharge voltage and good thermal stability, but the accessible capacity in the high-voltage region remains limited. In this work, conductive additives were introduced into $NiF_2$ by ethanol-assisted grinding or ultrasonic dispersion. Ag, Co, Ni, Sn, and graphene were first compared at an additive content of 10 wt%, followed by optimization of the Sn content. X-ray diffraction confirmed that $NiF_2$ was the major crystalline phase after dehydration and heat treatment and that metallic Sn remained detectable in the Sn-containing composite. Scanning electron microscopy showed fewer large agglomerated regions and a more dispersed particulate morphology for the ultrasonically treated sample. Using a LiB anode and a LiCl-LiBr-LiF-based electrolyte, the 10 wt% Sn-modified $NiF_2$ cathode delivered an initial voltage of 2.41 V and a specific capacity of 262.86 mAh $g^{-1}$ to a cutoff voltage of 2.0 V at 540°C and 100 mA $cm^{-2}$. Under the same conditions, pristine $NiF_2$ delivered 124.67 mAh $g^{-1}$, corresponding to an increase of approximately 110.8%. The 5 and 15 wt% Sn samples delivered 204.89 and 233.33 mAh $g^{-1}$, respectively, indicating a non-monotonic composition-performance relationship. These results show that an appropriate Sn content and dispersion route can substantially increase the accessible capacity of $NiF_2$ above 2.0 V.


# 1 Introduction

Thermal batteries are primary reserve power sources that use molten salts as electrolytes and are activated by heating. They are characterized by long storage life, rapid delivery of high power after activation, and good adaptability to high-temperature environments, making them suitable for applications that require long-term storage and rapid power output [1]. With the continuing development of thermal batteries toward higher specific energy, higher power, and miniaturization, cathode materials are required not only to provide a high operating voltage but also to maintain adequate stability and reaction kinetics in molten-salt environments [2].

$FeS_2$ is one of the most widely used cathode materials for thermal batteries because of its availability and mature processing technology. Nevertheless, voltage spikes, polarization, and limited thermal stability may still affect its discharge behavior at high temperature [3]. Transition-metal halides generally provide relatively high electrode potentials. Among them, $NiF_2$ has been investigated as a high-voltage cathode material for thermal batteries and has shown promising specific-power characteristics [4]. A major limitation of $NiF_2$ is its low intrinsic electronic conductivity, which can restrict charge transport and reduce the accessible discharge capacity under practical conditions. Related studies on $FeF_3$ have also demonstrated the potential of transition-metal fluorides as high-voltage thermal-battery cathodes and the usefulness of conductive carbonaceous components for improving electrode performance [5].

Introducing a conductive phase is a straightforward strategy for improving charge transport in composite cathodes [6, 7]. Metallic powders and carbon materials can both be used as conductive additives, but their effectiveness depends on the additive type, dispersion route, and loading. Insufficient

additive content may provide limited interparticle contact, whereas excessive addition can reduce the fraction of $NiF_2$ in the composite and may alter the structural behavior of the cathode at high temperature. For $NiF_2$, polypyrrole-derived N-doped carbon nanoparticles have recently been reported to improve discharge performance [8]. Conductive-carbon modification has also been applied to other thermal-battery cathodes, including $CoS_2$/CNT composites [9], carbon-coated $NiCl_2$ [10], and hierarchically carbon-modified nano-$NiS_2$ [11]. These studies indicate that the design of a conductive phase should be evaluated for the specific cathode chemistry and high-temperature operating conditions.

In the present work, two mixing routes, ethanol-assisted grinding and ultrasonic dispersion, were compared for $NiF_2$-based cathodes. Ag, Co, Ni, Sn, and graphene were screened as conductive additives at the same loading, after which the Sn content was varied from 5 to 15 wt%. Particular attention was paid to the accessible capacity above 2.0 V and to the relationship between initial voltage and high-voltage discharge capacity. The purpose of this study is therefore to establish a clear processing-composition-performance relationship for metallic Sn addition to $NiF_2$ cathodes without assigning a mechanism beyond that supported by the available structural and electrochemical evidence.

## 2 Materials and methods

# 2.1 Preparation of $NiF_2$-based cathode materials

$NiF_2 \cdot 4H_2O$ was used as the precursor. The powder was uniformly spread on a mica plate and heated at 180°C for 3 h to remove crystal water. After cooling, the powder was immediately sealed and transferred to a glove box. Before conductive-additive treatment, the resulting $NiF_2$ powder was dried again under vacuum at 180°C for 3 h to minimize the influence of moisture uptake during subsequent mixing and heat treatment.

# 2.1.1 Ethanol-assisted grinding

The dried $NiF_2$ powder was placed in an agate mortar, mixed with anhydrous ethanol and the required amount of conductive additive, and ground for 20 min. For additive screening, Ag, Co, Ni, Sn, and graphene were each added at 10 wt%. For optimization of the Sn content, 5, 10, and 15 wt% Sn were used. The mixture was maintained in a water bath at 85°C for 1 h to remove ethanol and was then ground again until homogeneous.

The resulting powder mixture was uniformly spread on carbon paper and heat-treated in a tube furnace under a continuous flow of high-purity Ar. According to the original experimental procedure, the temperature program consisted of holding at 70°C for 1 h, 500°C for 1 h, and 680°C for 1 h. After furnace cooling to room temperature, the sample was immediately sealed, transferred into the glove box, and ground for 20 min for subsequent cathode preparation.

# 2.1.2 Ultrasonic dispersion

The dried $NiF_2$ powder and the required amount of conductive additive were added to anhydrous ethanol and ultrasonically dispersed in a sealed container for 30 min. The suspension was then heated in a water bath at 85°C for 1 h to remove ethanol, and the recovered powder was ground until uniform. The same Ar-protected heat-treatment procedure used for the ethanol-assisted grinding route was then applied. After cooling, the powder was sealed and ground again in the glove box. Except for the mixing route, the additive loading, heat-treatment conditions, and subsequent cell-testing conditions were kept unchanged.

## 2.2 Materials characterization

The phase composition of the samples was examined by X-ray diffraction (XRD), and the particle morphology and dispersion state under different treatment conditions were observed by field-emission scanning electron microscopy (FESEM).

## 2.3 Single-cell assembly and discharge testing

Single cells were assembled in a glove box filled with high-purity Ar. The modified $NiF_2$ cathode material was mixed and ground with 15 wt% ternary all-lithium eutectic electrolyte powder and then pressed into a cathode pellet in a stainless-steel cell shell with a diameter of 15 mm at 10 MPa. A LiB alloy sheet was used as the anode. On the anode side, electrolyte powder containing 50 wt% MgO as a molten-salt immobilizer was added and pressed into an anode/electrolyte composite pellet in a cell shell with a diameter of 21 mm at 15 MPa. The single cell was assembled by stacking the cathode, electrolyte, and anode. LiCl-LiBr-LiF is a widely investigated all-lithium molten-salt electrolyte system for thermal batteries [12], while MgO is commonly used to retain molten electrolyte and suppress flow at elevated temperature [13].

Galvanostatic discharge tests were performed using a LAND battery testing system with the cells heated in a tube furnace under continuous Ar protection. Unless a specific experimental variable was being examined, comparative tests were conducted at 540°C and a current density of 100 mA $cm^{-2}$, with a cutoff voltage of 2.0 V. The specific-capacity values reported in this manuscript were normalized to the total mass of the cathode mixture, including $NiF_2$, the conductive additive when present, and the 15 wt% electrolyte component.

# 3 Results

## 3.1 Phase composition

The XRD patterns of the $NiF_2{\cdot}4H_2O$ precursor and the Sn-containing sample after dehydration and heat treatment are shown in Fig. 2. The precursor exhibits hydrate-related reflections, including prominent peaks in the low-angle region. After dehydration, Sn addition, and heat treatment, the major reflections can be assigned to anhydrous $NiF_2$, while additional diffraction signals corresponding to metallic Sn are

also observed. These results confirm the coexistence of crystalline $NiF_2$ and metallic Sn after the applied processing route.

It should be noted that the two patterns in Fig. 2 do not constitute a heat-treatment-matched control: the precursor is $NiF_2 \cdot 4H_2O$, whereas the Sn-containing sample has undergone dehydration and high-temperature treatment. Therefore, changes in peak positions, intensities, or apparent crystallinity cannot be attributed solely to Sn addition. The present XRD data are used only to establish the phase identity of the processed $NiF_2$/Sn composite.

# 3.2 Morphology

The $NiF_2$-based powders show distinct particle morphologies under different processing conditions (Fig. 3). The untreated $NiF_2 \cdot 4H_2O$ contains relatively large agglomerated particles, while dehydration and heat treatment alter the particulate morphology. For the samples containing 10 wt% Sn, fewer large agglomerated regions and a more dispersed particulate morphology are observed after ultrasonic dispersion than after ethanol-assisted grinding.

Ultrasonic treatment has been reported to promote de-agglomeration and dispersion of particles in liquid media [14]. In the present system, ultrasonic dispersion may therefore improve the dispersion state of the composite powder during liquid-phase mixing and consequently modify particle contact after heat treatment. However, because elemental mapping was not performed, the SEM images alone do not establish the spatial distribution of Sn.

# 3.3 Discharge performance

# 3.3.1 Effect of the mixing route

As shown in Fig. 4a, the two mixing routes produce clearly different discharge behavior when the Sn content is fixed at 10 wt% and the remaining test conditions are kept unchanged. The ethanol-ground sample shows an initial voltage of approximately 2.31 V and delivers 220.00 mAh $g^{-1}$ to 2.0 V. In comparison, the ultrasonically dispersed sample exhibits an initial voltage of 2.41 V and a capacity of 262.86 mAh $g^{-1}$. Based on the reported values, ultrasonic dispersion increases the capacity to the 2.0 V cutoff by approximately 19.5% relative to ethanol-assisted grinding. The main difference between the curves appears in the retention of the high-voltage discharge region, indicating that the mixing route strongly affects the accessible capacity at a fixed Sn content. The reduction in large agglomerated regions observed by SEM may be associated with this behavior, although the available evidence does not identify a unique charge-transport mechanism.

# 3.3.2 Effect of conductive-additive type

Figure 4b compares the discharge behavior of $NiF_2$ cathodes containing 10 wt% Ag, graphene, Co, Ni, or Sn. The initial voltages are 2.47, 2.41, 2.36, 2.34, and 2.41 V, respectively, while the corresponding

capacities to 2.0 V are 154.00, 152.00, 209.35, 247.10, and 262.86 mAh $g^{-1}$. The Ag-containing cathode exhibits the highest initial voltage, but its accessible capacity above 2.0 V is relatively low. In contrast, the Sn-containing cathode does not show the highest initial voltage, yet it delivers the largest capacity among the five conductive additives examined. These results indicate that the effectiveness of a conductive additive in this $NiF_2$ system cannot be evaluated from the initial voltage alone; the duration of the high-voltage region and the accessible capacity to the cutoff voltage must also be considered.

# 3.3.3 Effect of Sn content

A non-monotonic composition-performance relationship is observed when the Sn content is varied, as shown in Fig. 4c and d. The initial voltages of pristine $NiF_2$ and the 5, 10, and 15 wt% Sn samples are 2.48, 2.32, 2.41, and 2.25 V, respectively, and the corresponding capacities to 2.0 V are 124.67, 204.89, 262.86, and 233.33 mAh $g^{-1}$. Increasing the Sn content from 0 to 5 and 10 wt% progressively increases the accessible capacity. The 10 wt% Sn sample delivers approximately 110.8% more capacity than pristine $NiF_2$ under the same test conditions. When the Sn content is further increased to 15 wt%, however, the capacity decreases to 233.33 mAh $g^{-1}$, demonstrating that the benefit of Sn addition is not simply proportional to its loading.

Figure 4d compares the initial voltage and capacity to 2.0 V on the same composition axis. Pristine $NiF_2$ exhibits the highest initial voltage (2.48 V) but the lowest cutoff capacity, whereas the 10 wt% Sn sample has a slightly lower initial voltage (2.41 V) but the highest accessible capacity. Therefore, the principal experimental feature of Sn modification in this study is the increase in usable high-voltage capacity rather than an increase in the initial voltage.

Table 1
Quantitative summary of the discharge performance of $NiF_2$ cathodes under different modification conditions

| Comparison | Sample/condition | Initial voltage (V) | Peak voltage (V) | Capacity to 2.0 V (mAh $g^{-1}$) | Relative capacity change | Directly supported observation |
|---|---|---|---|---|---|---|
| Baseline | Pristine $NiF_2$ | 2.48 | — | 124.67 | — | Baseline under the same test conditions |
| Mixing route | 10 wt% Sn, ethanol grinding | 2.31 | — | 220.00 | + 76.5%* | Lower capacity than the ultrasonically dispersed sample |
| Mixing route | 10 wt% Sn, ultrasonic dispersion | 2.41 | 2.45 | 262.86 | + 110.8%* | ~ 19.5% higher capacity than ethanol grinding |
| Additive | 10 wt% Ag | 2.47 | 2.52 | 154.00 | + 23.5%* | High initial/peak voltage but relatively low accessible capacity |
| Additive | 10 wt% graphene | 2.41 | 2.49 | 152.00 | + 21.9%* | Low capacity to the 2.0 V cutoff |
| Additive | 10 wt% Co | 2.36 | 2.46 | 209.35 | + 67.9%* | Intermediate capacity |
| Additive | 10 wt% Ni | 2.34 | 2.46 | 247.10 | + 98.2%* | Higher capacity than the Co-containing sample |
| Additive | 10 wt% Sn | 2.41 | 2.45 | 262.86 | + 110.8%* | Highest capacity among the five additives examined |
| Sn content | 5 wt% Sn | 2.32 | 2.44 | 204.89 | + 64.3%* | Capacity clearly higher than pristine $NiF_2$ |
| Sn content | 10 wt% Sn | 2.41 | 2.45 | 262.86 | + 110.8%* | Highest capacity among the Sn |

| Comparison | Sample/condition | Initial voltage (V) | Peak voltage (V) | Capacity to 2.0 V (mAh $g^{-1}$) | Relative capacity change | Directly supported observation |
|---|---|---|---|---|---|---|
| | | | | | | contents examined |
| Sn content | 15 wt% Sn | 2.25 | — | 233.33 | + 87.2%* | Capacity decreases relative to 10 wt% Sn |

** Relative capacity changes were calculated using the pristine $NiF_2$ value of 124.67 mAh $g^{-1}$ as the baseline.*

# 4 Discussion

Under the same LiB anode, ternary all-lithium electrolyte, 540°C temperature, and 100 mA $cm^{-2}$ current density, the capacity of pristine $NiF_2$ to 2.0 V is 124.67 mAh $g^{-1}$, whereas the 10 wt% Sn-containing cathode delivers 262.86 mAh $g^{-1}$, corresponding to an increase of approximately 110.8%. At the same time, the initial voltage decreases slightly from approximately 2.48 V for pristine $NiF_2$ to 2.41 V for the 10 wt% Sn sample. This comparison reinforces that the primary benefit observed here is an increase in the accessible capacity above 2.0 V and a longer high-voltage discharge region rather than a higher initial voltage.

The structural characterization provides two direct observations. First, XRD confirms the coexistence of crystalline $NiF_2$ and metallic Sn after processing. Second, SEM shows fewer large agglomerated regions and a more dispersed particulate morphology for the ultrasonically treated sample. These observations are consistent with the improved discharge behavior, but they do not by themselves demonstrate the formation of a continuous Sn conductive network or quantify a reduction in charge-transfer or ohmic resistance.

The maximum heat-treatment temperature used in this work, 680°C, is substantially higher than the melting point of Sn (~ 232°C) [15]. Thus, Sn may melt and redistribute during heat treatment, which could influence the particle-contact state after cooling. This interpretation should be regarded as a plausible processing-related explanation rather than direct evidence of the structure present during thermal-battery operation. In addition, the electrochemical behavior of metal-fluoride electrodes can involve complex conversion reactions and phase evolution [16], and the present data do not allow the individual contributions of electronic transport, local contact, or possible chemical interactions to be separated.

The non-monotonic dependence on Sn content further indicates that the effect of Sn cannot be described as a simple linear function of additive loading. The 5 wt% sample performs below the 10 wt% sample, while increasing the Sn content to 15 wt% decreases the capacity from 262.86 to 233.33 mAh $g^{-1}$. Increasing the Sn fraction necessarily changes the composition of the composite cathode and may

also affect the local contact and redistribution behavior at elevated temperature. Among the compositions examined in this study, 10 wt% Sn provides the highest accessible capacity to 2.0 V.

## 5 Conclusions

Metallic conductive additives were introduced into $NiF_2$ cathodes using ethanol-assisted grinding and ultrasonic dispersion, and the effects of Ag, Co, Ni, Sn, and graphene were compared. XRD confirmed the coexistence of crystalline $NiF_2$ and metallic Sn after dehydration and heat treatment. SEM showed fewer large agglomerated regions and a more dispersed particulate morphology for the ultrasonically treated 10 wt% Sn sample than for the ethanol-ground counterpart. At a 2.0 V cutoff, ultrasonic dispersion increased the capacity of the 10 wt% Sn cathode from 220.00 to 262.86 mAh $g^{-1}$, corresponding to an increase of approximately 19.5%.

Among the five conductive additives examined at 10 wt%, Sn provided the highest capacity to 2.0 V. Increasing the Sn content from 5 to 10 wt% increased the capacity from 204.89 to 262.86 mAh $g^{-1}$, while a further increase to 15 wt% reduced it to 233.33 mAh $g^{-1}$, indicating a non-monotonic composition-performance relationship. At 540°C and 100 mA $cm^{-2}$, the 10 wt% Sn sample delivered an initial voltage of 2.41 V and a capacity of 262.86 mAh $g^{-1}$ to 2.0 V, approximately 110.8% higher than the pristine $NiF_2$ value of 124.67 mAh $g^{-1}$. Because pristine $NiF_2$ exhibits a higher initial voltage, the main advantage of Sn addition in the present study is the increase in accessible high-voltage capacity rather than an increase in initial voltage.

## Declarations

# Competing interests:

The authors declare no competing interests.

# Funding:

No funding was received for this work.

# Author Contribution

M.S. performed the experiments and analyzed the data. S.Y. and H.W. provided guidance on the experimental work. Z.D. supervised the overall research and reviewed and revised the manuscript. All authors reviewed and approved the final manuscript.

# Data availability:

The data that support the findings of this study are available from the corresponding author upon reasonable request.

## References


1. Guidotti RA, Masset P (2006) Thermally activated (thermal) battery technology. J Power Sources 161:1443–1449. https://doi.org/10.1016/j.jpowsour.2006.06.013
2. Li R, Guo W, Qian Y (2022) Recent developments of cathode materials for thermal batteries. Front Chem 10:832972. https://doi.org/10.3389/fchem.2022.832972
3. Masset PJ, Guidotti RA (2008) Thermal activated (thermal) battery technology: Part IIIa: $FeS_2$ cathode material. J Power Sources 177:595–609. https://doi.org/10.1016/j.jpowsour.2007.11.017
4. Chang Q, Luo Z, Fu L, Zhu J, Yang W, Li D, Zhou L (2020) A new cathode material of $NiF_2$ for thermal batteries with high specific power. Electrochim Acta 361:137051. https://doi.org/10.1016/j.electacta.2020.137051
5. Guo SN, Guo H, Wang X, Zhu Y, Hu J, Yang M, Zhao L, Wang J (2019) Iron trifluoride as a high voltage cathode material for thermal batteries. J Electrochem Soc 166:A3599–A3605. https://doi.org/10.1149/2.0371915jes
6. Tian Q, Wang J, Xiang W, Zhao J, Guo H, Hu J, Han X, Hu W (2021) Fabrication of the Ni–$NiCl_2$ composite cathode material for fast-response thermal batteries. Front Chem 9:679231. https://doi.org/10.3389/fchem.2021.679231
7. Choi Y, Cho S, Lee YS (2014) Effect of the addition of carbon black and carbon nanotube to $FeS_2$ cathode on the electrochemical performance of thermal battery. J Ind Eng Chem 20:3584–3589. https://doi.org/10.1016/j.jiec.2013.12.052
8. Qiao S, Kang M, Zhao Z, Wang X, Fan Z, Wu Q, Xiang B (2025) Polypyrrole-derived N doped carbon nanoparticle as addictive for high-performance thermal batteries with $NiF_2$ electrode. Mater Lett 384:138121. https://doi.org/10.1016/j.matlet.2025.138121
9. Xie S, Deng Y, Mei J, Yang Z, Lau WM, Liu H (2016) Facile synthesis of $CoS_2$/CNTs composite and its exploitation in thermal battery fabrication. Compos Part B Eng 93:203–209. https://doi.org/10.1016/j.compositesb.2016.03.038
10. Jin C, Zhou L, Fu L, Zhu J, Li D (2017) Synthesis and discharge performances of $NiCl_2$ by surface modification of carbon coating as cathode material of thermal battery. Appl Surf Sci 402:308–313. https://doi.org/10.1016/j.apsusc.2017.01.034
11. Jin C, Fu L, Zhu J, Yang W, Li D, Zhou L (2018) A hierarchical carbon modified nano-$NiS_2$ cathode with high thermal stability for a high energy thermal battery. J Mater Chem A 6:7123–7132. https://doi.org/10.1039/C8TA00346G
12. Masset P, Guidotti RA (2007) Thermal activated (thermal) battery technology: Part II. Molten salt electrolytes. J Power Sources 164:397–414. https://doi.org/10.1016/j.jpowsour.2006.10.080

13. Masset P, Schoeffert S, Poinso JY, Poignet JC (2005) Retained molten salt electrolytes in thermal batteries. J Power Sources 139:356–365. https://doi.org/10.1016/j.jpowsour.2004.07.009
14. Sauter C, Emin MA, Schuchmann HP, Tavman S (2008) Influence of hydrostatic pressure and sound amplitude on the ultrasound induced dispersion and de-agglomeration of nanoparticles. Ultrason Sonochem 15:517–523. https://doi.org/10.1016/j.ultsonch.2007.08.010
15. National Institute of Standards and Technology (NIST) Tin: phase change data. NIST Chemistry WebBook, SRD 69. Accessed 10 September 2026. https://webbook.nist.gov/cgi/cbook.cgi?ID=C7440315&Mask=4
16. Wang F, Robert R, Chernova NA, Pereira N, Omenya F, Badway F et al (2011) Conversion reaction mechanisms in lithium ion batteries: study of the binary metal fluoride electrodes. J Am Chem Soc 133:18828–18836. https://doi.org/10.1021/ja206268a

## Figures

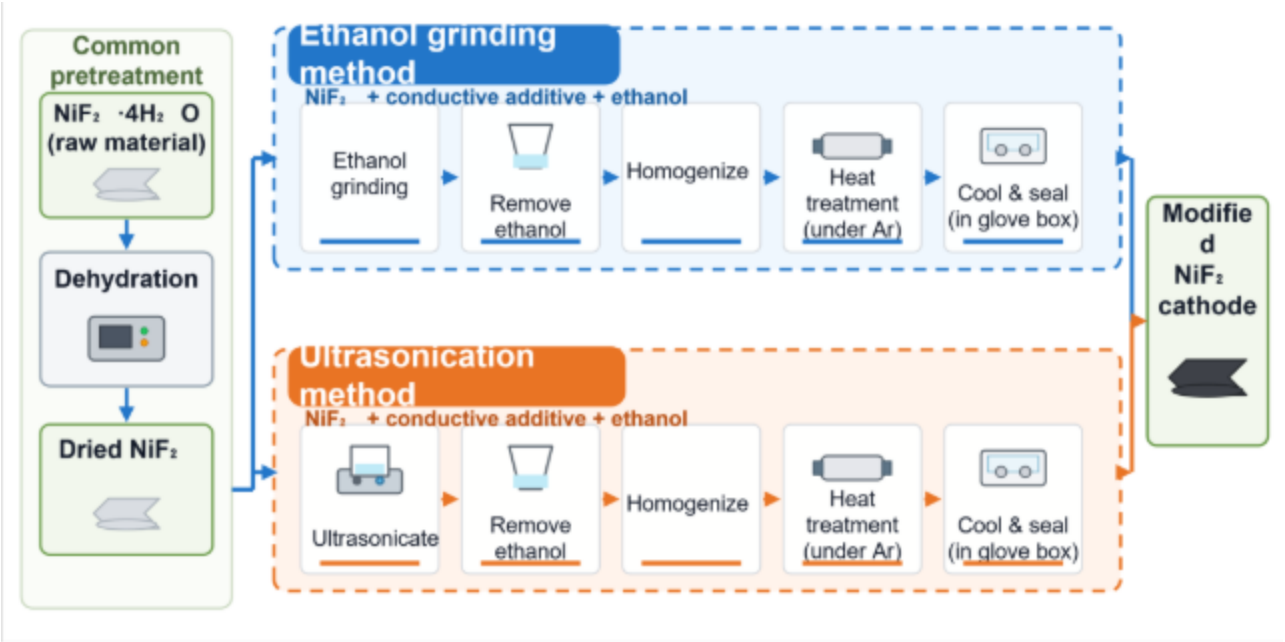


**Figure 1**

Preparation routes for Sn-modified $NiF_2$ cathode materials using ethanol-assisted grinding and ultrasonic dispersion

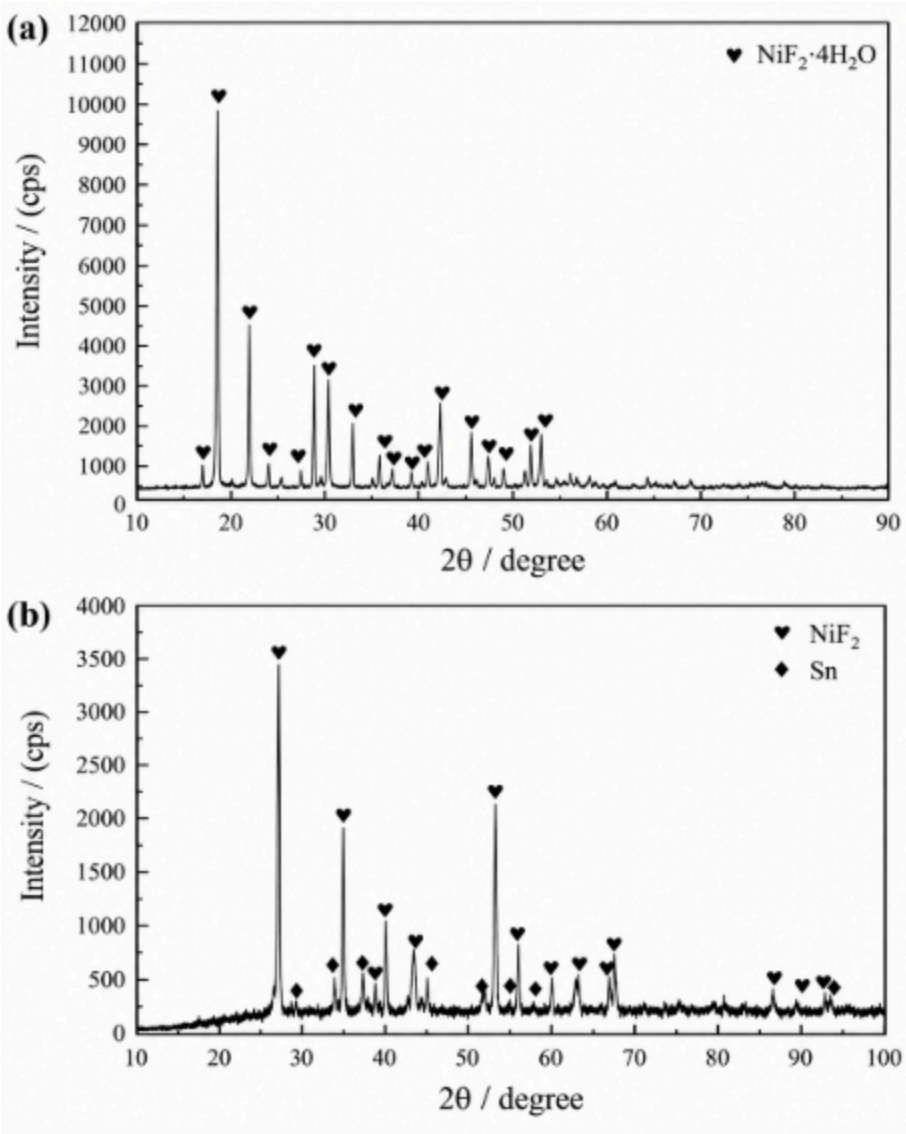


**Figure 2**

XRD patterns of (a) the $NiF_2 \cdot 4H_2O$ precursor and (b) the $NiF_2$/Sn sample after dehydration, addition of 10 wt% Sn, and heat treatment

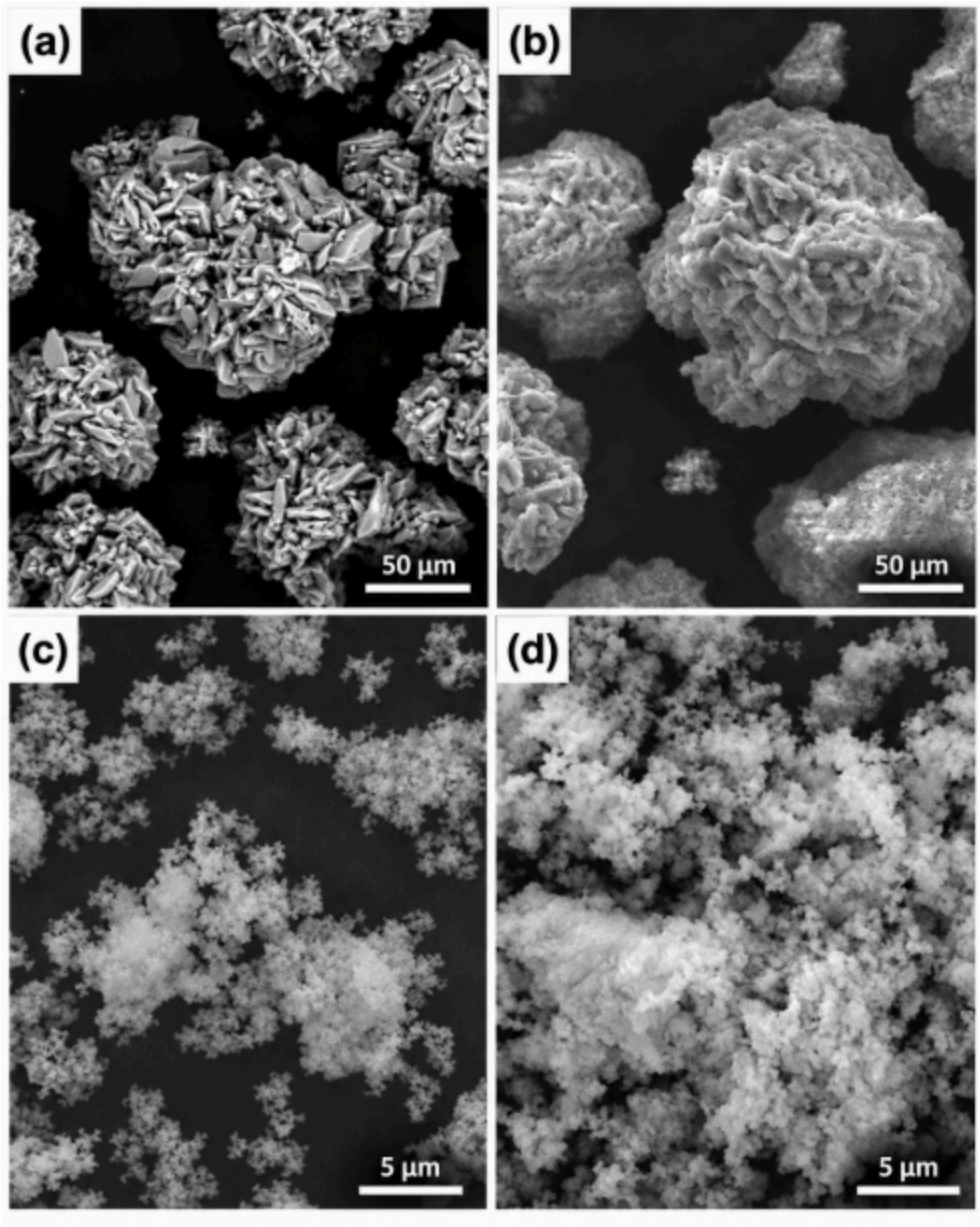


**Figure 3**

SEM images of $NiF_2$-based samples under different processing conditions: (a) $NiF_2 \cdot 4H_2O$, (b) dehydrated/heat-treated $NiF_2$, (c) 10 wt% Sn-containing $NiF_2$ prepared by ultrasonic dispersion, and (d) 10 wt% Sn-containing $NiF_2$ prepared by ethanol-assisted grinding

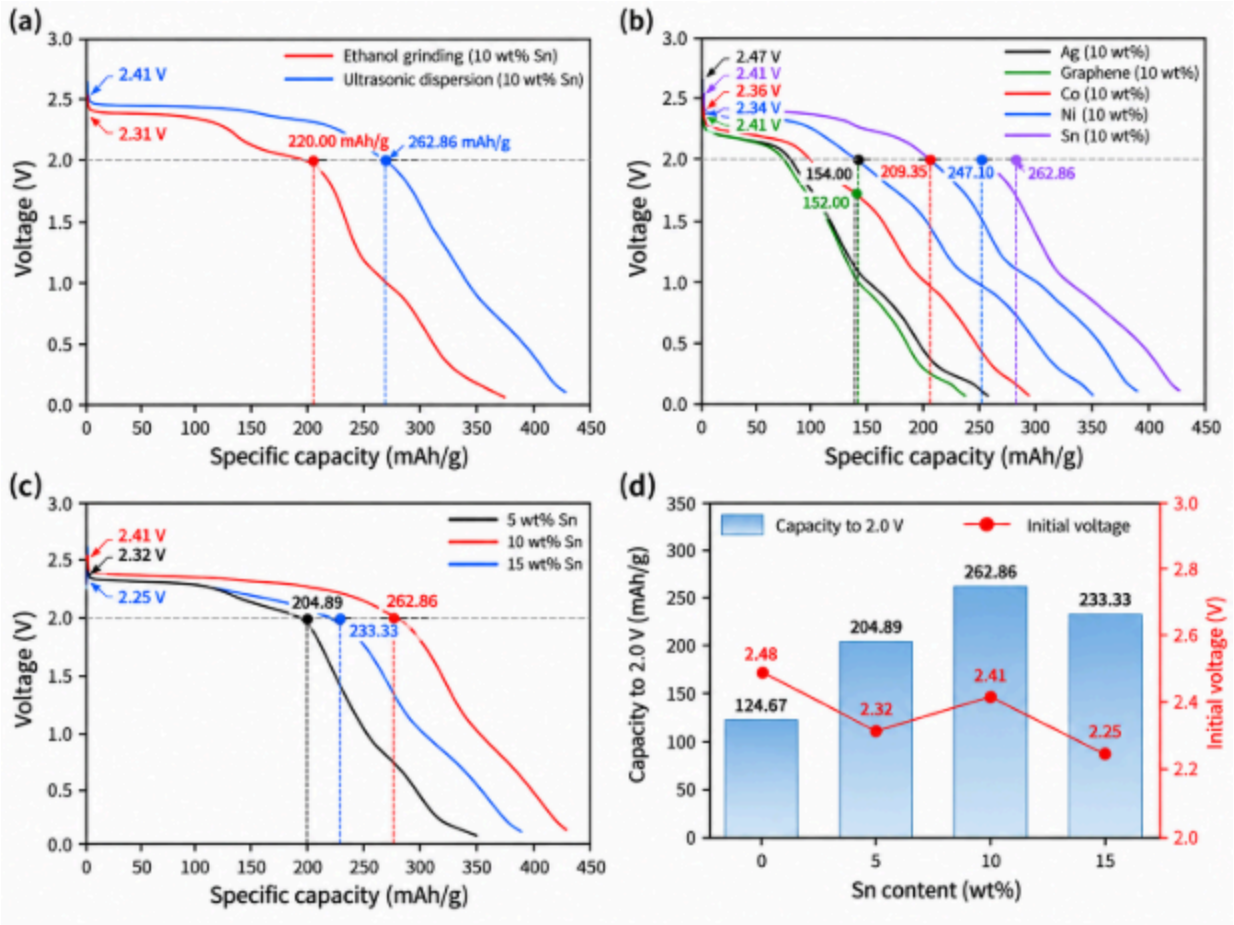


**Figure 4**

Systematic comparison of the discharge performance of Sn-modified $NiF_2$ cathodes: (a) different mixing routes for 10 wt% Sn, (b) different conductive additives at 10 wt%, (c) different Sn contents, and (d) effects of Sn content on the capacity to 2.0 V and initial voltage